

Article

Electrical Conductivity Based Ammonia Sensing Properties of Polypyrrole/MoS₂ Nanocomposite

Sharique Ahmad¹, Imran Khan¹, Ahmad Husain², Anish Khan^{3,4,*} and Abdullah M. Asiri^{3,4,*}

¹ Applied Science and Humanities Section, University Polytechnic, Faculty of Engineering and Technology, Aligarh Muslim University, Aligarh 202002, India; shariqueahmad14@gmail.com (S.A.); imrannano@gmail.com (I.K.)

² Department of Applied Chemistry, Faculty of Engineering and Technology, Aligarh Muslim University, Aligarh 202002, India; ahmadhusain2065@gmail.com

³ Center of Excellence for Advanced Materials Research, King Abdulaziz University, Jeddah 21589, Saudi Arabia

⁴ Chemistry Department, Faculty of Science, King Abdulaziz University, Jeddah 21589, Saudi Arabia

* Correspondence: anishkhan97@gmail.com (A.K.); aasiri2@kau.edu.sa (A.M.A.)

Received: 25 November 2020; Accepted: 15 December 2020; Published: 18 December 2020



Abstract: Polypyrrole (PPy) and Polypyrrole/MoS₂ (PPy/MoS₂) nanocomposites were successfully prepared, characterized and studied for ammonia sensing properties. The as-prepared PPy and PPy/MoS₂ nanocomposites were confirmed by FTIR (Fourier transform infrared spectroscopy), XRD (X-ray diffraction), SEM (scanning electron microscopy) and TEM (transmission electron microscopy) techniques. The ammonia sensing properties of PPy and PPy/MoS₂ nanocomposites were studied in terms of change in DC electrical conductivity on exposure to ammonia vapors followed by ambient air at room temperature. It was observed that the incorporation of MoS₂ in PPy showed high sensitivity, significant stability and excellent reversibility. The enhanced sensing properties of PPy/MoS₂ nanocomposites could be attributed to comparatively high surface area, appropriate sensing channels and efficiently available active sites. The sensing mechanism is explained on the basis of simple acid-base chemistry of polypyrrole.

Keywords: nanocomposite; polypyrrole/MoS₂; ammonia sensing; electrical conductivity

1. Introduction

A new era began in the field of polymers after the discovery of conductivity in polyacetylene by Shirakawa et al. [1]. Over the years, the field of conducting polymers has seen a great extent of research been carried out since it first came to light that conjugated polymers could be made to conduct by the process of doping. They have aroused great interest since then and have been employed to fabricate sensing devices as their electrical and electrochemical properties can easily and precisely be altered according to necessities [2–10]. In recent times, conducting polymers such as polythiophene (PTh), polypyrrole (PPy) and polyaniline (Pani) have been extensively used for the fabrication of gas and vapor sensors [2–4,8–15]. Among the several conducting polymers available nowadays, polypyrrole (PPy) and its composite materials have attracted attention as it is easy to synthesize, possesses high conductivity and is environmentally stable [6,9].

It is well-recognized that amalgamating polypyrrole with inorganic nanomaterials results in the formation of nanocomposites which are environmentally and chemically more stable than pristine PPy [6,9,12]. DC electrical conductivity and gas/vapor sensing properties of PPy can be significantly enhanced by the formation of its nanocomposites [12]. Usually, these nanocomposites have been synthesized by the oxidative chemical polymerization method and have been used for detecting a

number of gases and volatile organic compounds (VOCs). The sensors based on conductive polymers (CPs) such as polypyrrole (PPy) offer great advantages, such as they are highly sensitive, have shorter response time and can operate at room temperature. These sensors display excellent sensing ability due to the synergistic effect of both the components, i.e., PPy and nano-fillers [6,9,12,16–18].

Herein, molybdenum disulfide (MoS_2) is employed as a nano-filler in order to synthesize PPy/ MoS_2 nanocomposites for enhancing electrical and ammonia sensing properties of pristine PPy. Since its discovery by Tenne et al., MoS_2 nanoparticles have been established as an outstanding material in electronics, optoelectronics and sensor chemistry due to its low band gap (1.8 eV) and thermal and chemical stability [19–26]. Therefore, MoS_2 nanoparticles are utilized as a nano-filler for the preparation of conducting polymers' nanocomposites. The incorporation of MoS_2 nanoparticles into polymer matrix enhanced the electrical, optical, thermal and mechanical properties of polymers [5,27–29].

Among the various toxic gases/vapors, ammonia is the most commonly produced from vehicular emissions and various industries. It is very harmful if inhaled in large amounts, usually greater than 300 ppm, and may damage human body cells and various respiratory diseases. It may also cause various problems to human health such as sore throat, headache, chest pain, fatigue, vomiting, etc. Therefore, detection of ammonia at ppm levels is compulsory for the assessment of human health [2,4,16,17]. Conducting polymer-based materials have been utilized for the fast and selective detection of ammonia in the form of pellet-shaped sensors. Husain et al. fabricated a pellet-shaped ammonia sensor utilizing polythiophene/ multi walled carbon nanotubes and polythiophene/ single walled carbon nanotubes (PTh/MWCNT and PTh/SWCNT) nanocomposites which can detect it selectively at an extremely low concentration of 0.1 and 0.5 ppm, respectively [16,17]. Ahmad et al. reported a novel pellet-shaped ammonia sensor based on Pani/nickel oxide/graphene nanocomposites with lower detection limit of 170 ppm at room temperature [30].

Niaz et al. [31] successfully prepared a MoS_2 /PPy nanocomposite by the in-situ oxidative polymerization method. They evaluated its electrochemical properties for possible application in supercapacitors as electrode materials. The results showed that the MoS_2 /PPy nanocomposite electrode exhibited very high specific capacitance (654 Fg⁻¹) along with 95% retention of performance, even after 500 cycles. Lian et al. [32] also utilized a PPy/ MoS_2 nanocomposite for the fabrication of electrode materials in supercapacitors. The results revealed that the electrode possesses an exceptionally high specific capacitance (895.6 Fg⁻¹) as well as outstanding cycling stability of about 98% after 10,000 cycles. In another study, Lei et al. [33] synthesized the MoS_2 /PPy nanocomposite by the hydrothermal method. They reported that the MoS_2 /PPy nanocomposite showed greater peroxidase-like catalytic action towards oxidation of 3,3,5,5-tetramethylbenzidine (TMB) in the presence of hydrogen peroxide in acetate buffer solution. The catalytic performance of the MoS_2 /PPy nanocomposite was found to be superior to the pure PPy and MoS_2 .

Papadopoulou et al. synthesized a polyimide-based real-time ammonia sensor by measuring the changes in the electric current intensity with concentration as low as 3.5 mM [34].

To the best of our knowledge, this is the first report on ammonia sensing studies of the PPy/ MoS_2 nanocomposite. Thus, we firmly believe that this study will contribute significantly towards the fabrication of a highly sensitive, completely reversible and very selective gas/vapor sensor working at room temperature.

In this study, we have prepared pristine PPy and nanocomposites of PPy having 20 wt.% of MoS_2 with respect to the weight of pyrrole (monomers). The successful formation of PPy and PPy/ MoS_2 nanocomposites have been confirmed by FTIR, XRD, SEM and TEM techniques. Electrical and ammonia sensing properties of the materials were studied at room temperature.

2. Materials, Methods and Instrumentation

2.1. Materials

Pyrrole 99% (Sigma-Aldrich, St. Louis, MI, USA), molybdenum disulfide (MoS_2) (CDH, India), anhydrous ferric chloride (Fischer scientific India) and methanol (Fischer scientific India) were used. We used double-distilled water in the experiments.

2.2. Instrumentation

FTIR (Fourier transform infrared spectroscopy) was performed on different samples between a wavenumber range of $4000\text{--}400\text{ cm}^{-1}$ by the spectrophotometer Nicolet (Model iS50, Thermo Scientific, Berkeley, MI, USA) with a built-in ATR (Attenuated Total Reflectance) accessory. The JEOL model (JSM-7600F, JEOL, Tokyo, Japan).JSM-7600F was used for scanning electron microscopy (SEM) photographs' collection, while the transmission electron microscopy (TEM) images were collected through the instrument JEOL model (JEM-6510LV, JEOL, Japan). XRD patterns of the solids were recorded at room temperature (RT) by a Thermo-Scientific powder diffractometer instrument (model ARL X'TRA, Thermo Scientific, Berkeley, MI, USA). The angle of the diffractometer was kept at a 2θ range from 10 to 80° , while the scanning rate was 0.002°s^{-1} with a Copper $\text{K}\alpha$ radiation ($\lambda = 1.5418\text{ \AA}$).

2.3. Preparation of PPy and PPy/MoS₂ Nanocomposite

Polypyrrole (PPy) and PPy/ MoS_2 nanocomposites were prepared via the in-situ oxidative polymerization routine in the aqueous medium using anhydrous ferric chloride (FeCl_3) as the oxidant [9,12]. Firstly, a requisite amount of MoS_2 powder was added into a 500 mL beaker having 200 mL of double-distilled water, then ultra-sonicated for 4 h for the exfoliation of MoS_2 sheets. After that, 4.16 ml (0.06 mol) of pyrrole monomers were transferred into the beaker containing MoS_2 and further sonicated for 2 h for the adsorption of monomers on the surface of MoS_2 . Then, 9.72 g (0.06 mol) of anhydrous ferric chloride was added into a beaker containing 100 mL of double-distilled water and stirred for a few minutes. Afterward, the prepared aqueous solution of ferric chloride was transferred dropwise into the beaker containing pyrrole monomers and MoS_2 , along with continuous stirring for 10 h in order to achieve thorough polymerization of pyrrole. After polymerization, the nanocomposite was obtained as a black slurry which was filtered along with washing carefully with double-distilled water as well as methanol. Finally, washed and filtered material was dried in an oven at 70°C for 12 h and converted into powder for characterization. The pristine PPy nanoparticles have also been prepared by the same method for reference and comparison.

2.4. Characterization

The Perkin-Elmer-1725 instrument on KBr-pellets was used for recording FTIR spectra of PPy, MoS_2 and PPy/ MoS_2 . The morphology was determined by SEM and TEM images. The scanning electron microscopic studies were done to study the surface morphology by scanning a focused electron beam over the surface of the materials by JEOL, JSM, 6510-LV (JEOL, Japan). The transmission electron microscopic studies were done to study the detailed internal morphology of the material by JEM 2100, (JEOL, Japan). The crystalline and amorphous nature of the material was analyzed by X-rays diffraction patterns. XRD data of materials were recorded by a Bruker D8 diffractometer with Cu $\text{K}\alpha$ radiation at 1.540 \AA in the range of $5^\circ \leq 2\theta \leq 80^\circ$ at 50 kV.

DC electrical conductivity as well as ammonia sensing experiments were carried out with four in-line probe instruments attached with a PID (proportional integral derivative)-controlled oven manufactured by Scientific Equipment, Roorkee, India. The equation used for the calculation of DC electrical conductivity is given below:

$$\sigma = [\ln 2 (2S/W)]/[2\pi S (V/I)] \quad (1)$$

where I , V , W , S and σ represent the current (A), voltage (V), the thickness of the pellet (cm), probe spacing (cm) and conductivity ($S \cdot \text{cm}^{-1}$), respectively [11–13]. The pellets used in conductivity and sensing experiments were made by a hydraulic pressure machine at 70 kN pressure applied for 60 s. 250 mg of each sample was used for the preparation of pellets.

3. Results and Discussions

3.1. Fourier Transform Infrared Spectroscopic (FTIR) Studies

The FTIR spectra of PPy, MoS₂ and PPy/MoS₂ nanocomposites are depicted in Figure 1. The typical peaks of PPy observed at 1546 and 1460 cm^{-1} are due to C=C stretching vibrations, as shown in Figure 1a. The peaks at 1306, 1186 and 1042 cm^{-1} are related to the C=N bending, C–N stretching and =C–H bending vibrations of PPy, respectively. The two peaks at 788 and 678 cm^{-1} are attributed to C–H out of plane deformational vibration-mode of the PPy ring. The peak present at 922 cm^{-1} corresponds to the C=N⁺–C stretching vibration. This peak at 922 cm^{-1} confirms the doping of PPy by FeCl₃ and creation of charge carriers, i.e., polarons [6,7,9,12,31].

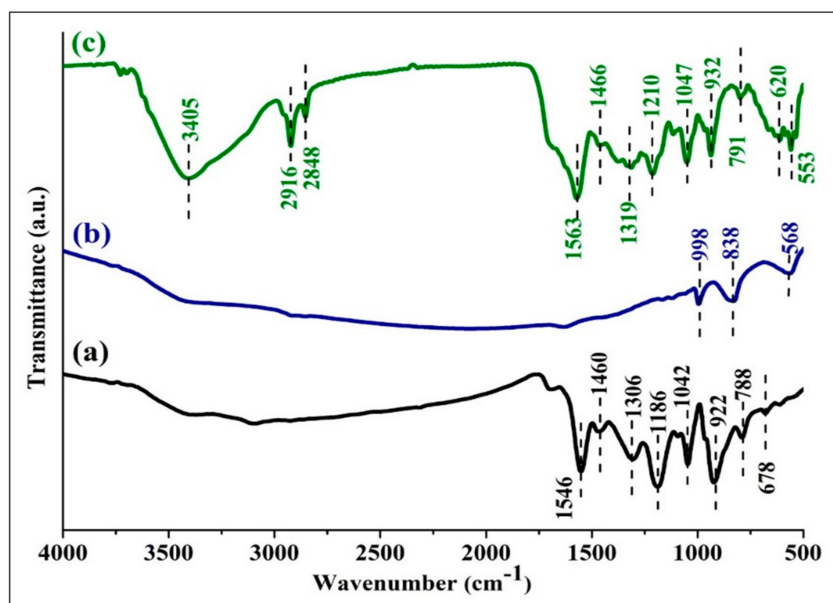


Figure 1. The Fourier transform infrared (FTIR) spectra of: (a) PPy, (b) MoS₂ and (c) PPy/MoS₂.

In the spectrum of MoS₂ (Figure 1b), the peaks witnessed at 998, 839 and 568 cm^{-1} are in good agreement with the existing literature. These peaks at 998 and 568 cm^{-1} may be assigned to the S–S and Mo–S bonds of MoS₂, respectively [5,22,23,31].

In the spectrum of PPy/MoS₂ (Figure 1c), the peaks at 3405, 2916 and 2848 cm^{-1} are due to the –OH group of moisture and stretching vibrations of C–H bonds, respectively. In the case of PPy/MoS₂, all the characteristic peaks of PPy can be seen, along with a new peak at 553 cm^{-1} which confirms the presence of MoS₂ in the nanocomposite. The peaks observed at 1546, 1460, 1306, 1186, 1042, 922 and 788 cm^{-1} in the spectrum of pristine PPy are observed at slightly higher wavenumbers in the case of PPy/MoS₂ at 1563, 1466, 1319, 1210, 1047, 932 and 791 cm^{-1} , respectively. The shifting of characteristic peaks of PPy in the spectrum of PPy/MoS₂ shows the electronic/synergistic interaction working at molecular levels [31,33].

3.2. X-ray Diffraction (XRD) Studies

The XRD spectra of PPy, MoS₂ and PPy/MoS₂ nanocomposites are depicted in Figure 2. In the spectrum of PPy (Figure 2a), the broad diffraction peak seen at $2\theta = 21\text{--}27^\circ$ shows the amorphous nature of PPy [9,12,31,32]. In the case of MoS₂ (Figure 2b), the peaks located at $2\theta = 32.65^\circ, 33.61^\circ, 35.90^\circ, 39.55^\circ, 44.20^\circ, 49.86^\circ, 56.15^\circ, 58.50^\circ$ and 60.35° are assigned to (100), (101), (102), (103), (006), (105), (106), (110), (008) and (108) diffraction planes, respectively [20,24,31]. Whereas in the spectrum PPy/MoS₂ (Figure 2c), the distinctive peaks of MoS₂ are detected at slightly higher angles, i.e., $2\theta = 32.78^\circ, 33.72^\circ, 35.99^\circ, 39.70^\circ, 44.30^\circ, 49.92^\circ, 56.26^\circ, 58.59^\circ$ and 60.65° respectively, displaying molecular interaction between PPy and MoS₂. The intensity of all the peaks of MoS₂ is decreased considerably in PPy/MoS₂, clarifying the successful and comprehensive coverage of MoS₂ sheets by the PPy matrix, which could be understood by SEM and TEM images of PPy/MoS₂.

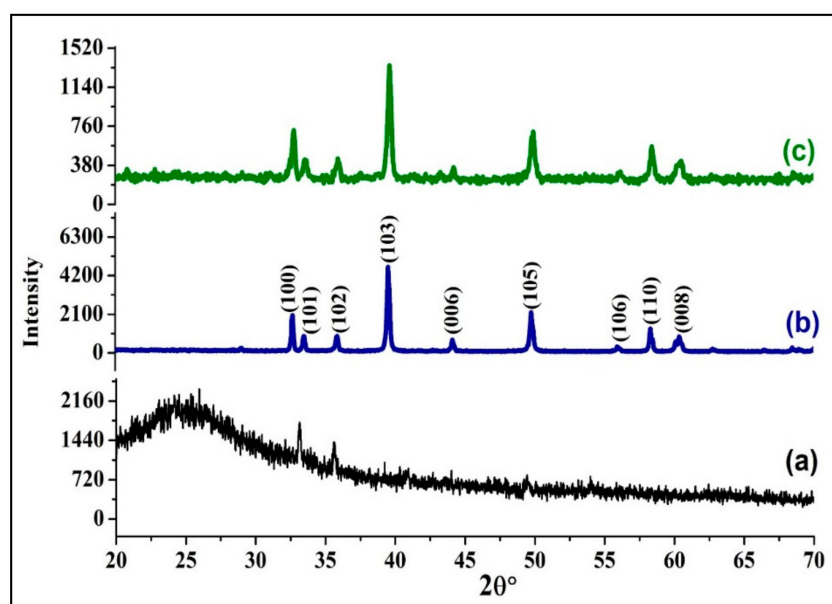


Figure 2. The X-ray diffraction (XRD) spectra of: (a) PPy, (b) MoS₂ and (c) PPy/MoS₂.

3.3. Morphological Studies

The SEM micrographs of pristine PPy, MoS₂ and PPy/MoS₂ nanocomposites together with the TEM image of PPy/MoS₂ are presented in Figure 3. The surface of pristine PPy (Figure 3a) consists of globular nanoparticles which are agglomerated with each other [12]. In the case of MoS₂ (Figure 3b), surface morphology is sheet-like. The SEM image of PPy/MoS₂ (Figure 3c) shows that pyrrole is successfully polymerized on the surface of MoS₂ nano-sheets. The size of globular nanoparticles of PPy/MoS₂ are greater than the size of pristine PPy. Some sheet-like structures are also observed in PPy/MoS₂, which confirms the presence of MoS₂ in nanocomposites on which pyrrole polymerized. The TEM image of PPy/MoS₂ is shown in Figure 3d.

3.4. DC Electrical Conductivity

DC electrical conductivity as well as ammonia sensing experiments were carried with four in-line probe instruments attached with a PID-controlled oven manufactured by Scientific Equipment, Roorkee, India. The schematic representation of instrument is shown below in Figure 4.

The initial DC electrical conductivities of MoS₂, PPy and PPy/MoS₂ nanocomposites were determined by a standard four in-line probes method, as shown in Figure 5. The electrical conductivities of MoS₂, PPy and PPy/MoS₂ nanocomposites at room temperature were observed to be 2.2×10^{-6} , 2.03 and $8.33 \text{ S}\cdot\text{cm}^{-1}$, respectively. The electrical conductivity of PPy/MoS₂ nanocomposites increases drastically after incorporation of MoS₂ into pure PPy. This sudden rise in electrical conductivity of

PPy/MoS₂ nanocomposites may be due to the interaction of lone pairs of nitrogen of polypyrrole with molybdenum of MoS₂ producing more holes in PPy, leading to a rise in electrical conductivity.

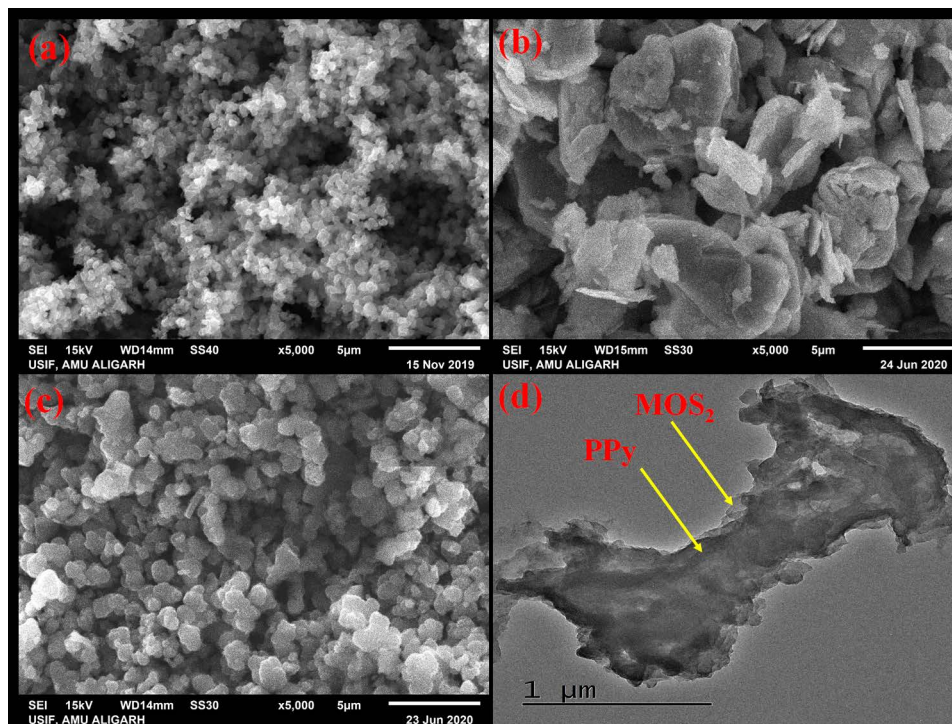


Figure 3. Scanning electron microscopy (SEM) micrographs of: (a) PPy, (b) MoS₂ (c) PPy/MoS₂ and (d) transmission electron microscopy (TEM) micrograph of PPy/MoS₂.

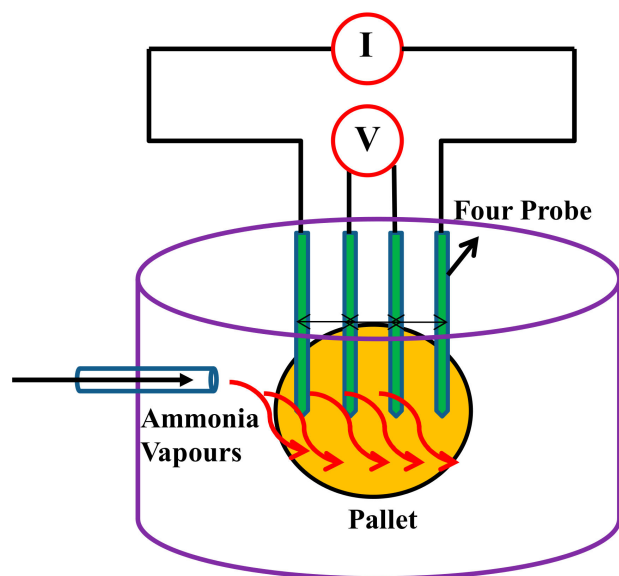


Figure 4. Ammonia sensor unit by the four in-line probes method.

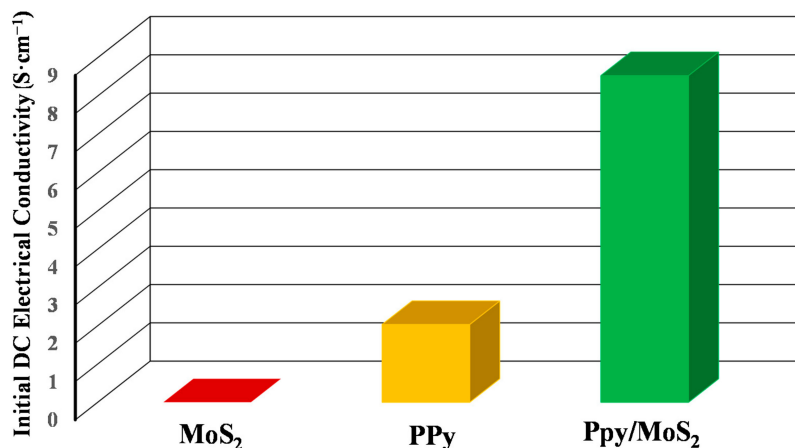


Figure 5. Initial DC electrical conductivities of MoS₂, PPy and PPy/MoS₂ nanocomposites.

3.5. Sensitivity

The sensitivities of PPy and PPy/MoS₂ towards ammonia vapors with time were studied as shown in Figure 6. Upon passing 1000 ppm of ammonia vapors to the surface of PPy/MoS₂, the DC electrical conductivity of PPy/MoS₂ decreased from 8.3719 to 0.9488 S·cm⁻¹ in 70 s and reached a steady-state level in ammonia atmosphere for 180 s. After 180 s, as the PPy/MoS₂ placed in ambient air, the DC electrical conductivity started to increase rapidly and resumed back to 7.5369 S·cm⁻¹ in the next 120 s. Similarly, in case of pristine PPy, the change in DC electrical conductivity was found to be very marginal upon exposure to 1000 ppm of ammonia. The excellent sensitivity of PPy/MoS₂ may be attributed to high surface area and active sites available for more adsorption and desorption for analyte gas.

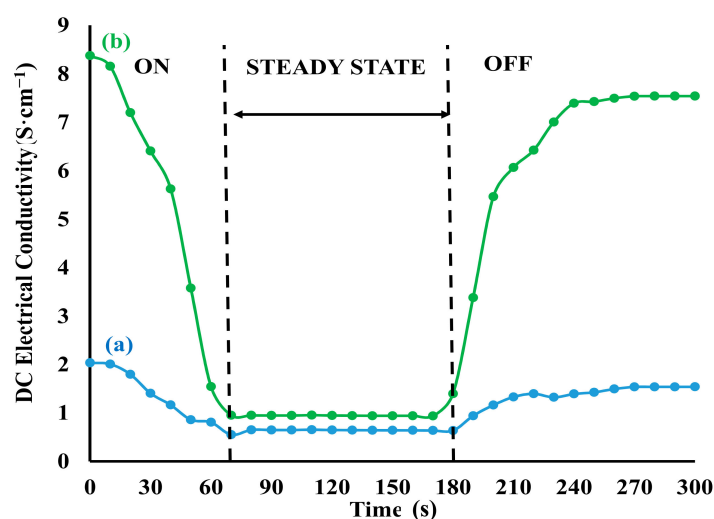


Figure 6. Effect on the DC electrical conductivity of (a) PPy and (b) PPy/MoS₂ nanocomposites upon exposure to (1000 ppm) ammonia vapors followed by exposure to ambient air with respect to time.

3.6. Limit of Detection

The PPy/MoS₂ nanocomposites were tested for limit of detection towards various concentrations of ammonia, as shown in Figure 7. As the concentration of ammonia decreased from 1000 to 300 ppm, the rate of change of conductivity also decreased and became minimized for the 300 ppm concentration of ammonia. Thus, the electrical conductivity change of PPy/MoS₂ nanocomposites could be observed in contact with ammonia as low as 300 ppm concentration.

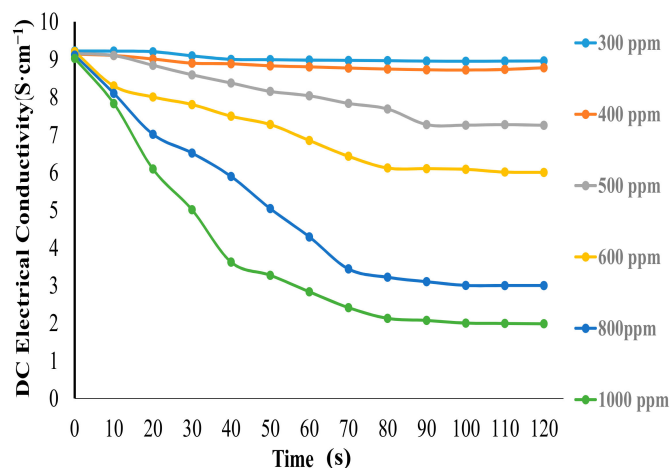


Figure 7. Effect on the DC electrical conductivity of the PPy/MoS₂ nanocomposites upon exposure to ammonia vapors at different concentrations.

3.7. Reversibility

The reversibility of PPy/MoS₂ nanocomposites and PPy was studied in terms of the DC electrical conductivity as the cycling between the analyte and ambient air without any loss in its sensing performance, as shown in Figure 8. The reversibility of PPy/MoS₂ nanocomposites and PPy was examined by first exposing the sample to 1000 ppm of ammonia vapors for 30 s, followed by 30 s in ambient air for a total duration of 150 s. Figure 8A shows the reversibility of PPy/MoS₂ nanocomposites with a fine repeated range of conductivity change from 9.145 to 6.488 S·cm⁻¹ in the ambient air and upon exposure to 1000 ppm of ammonia vapors, respectively. The overall conductivity change for PPy/MoS₂ nanocomposites was about 2.65 S·cm⁻¹. Figure 8B shows the reversibility of pure PPy, within the conductivity range of 1.79 to 1.848 S·cm⁻¹. The overall conductivity change for PPy was about 0.058 S·cm⁻¹, which is very nominal in comparison with PPy/MoS₂ nanocomposite. There were about 55 times better variations observed in conductivity of PPy/MoS₂ nanocomposite than that of pure PPy.

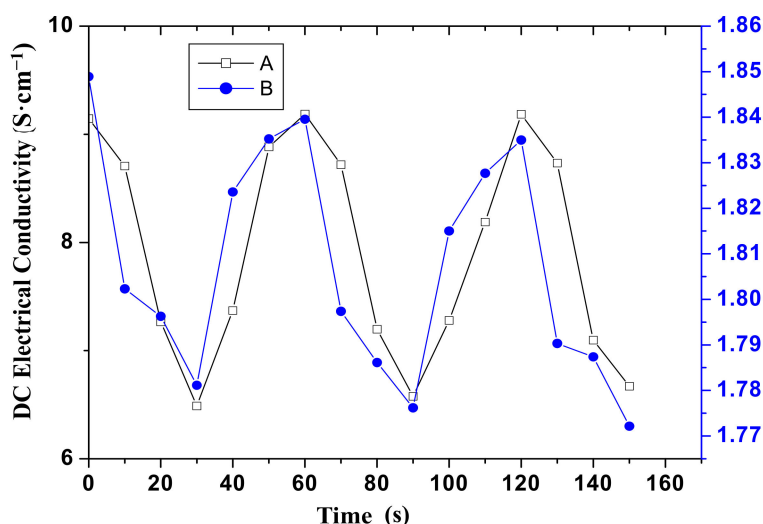


Figure 8. Electrical conductivity of curve A PPy/MoS₂ nanocomposite and curve B PPy upon alternate exposure to 1000 ppm of ammonia vapors and air with respect to time.

3.8. Selectivity

The DC electrical conductivity responses of PPy/MoS₂ nanocomposite towards ammonia and VOCs (volatile organic compounds) viz. ethanol, propanol, acetaldehyde, formaldehyde, diethyl ether

and phenol at room temperature ($\sim 27^\circ\text{C}$), are shown in Figure 9. It was observed that the PPy/MoS₂ nanocomposite showed the highest change in DC electrical conductivity towards 1000 ppm of ammonia among different analytes. Such a high selectivity of ammonia results from the highest electron donating tendency among the analytes tested. Therefore, the lesser electron-donating affinity of VOCs causes a lesser conductivity change. This also infers the higher selectivity of the PPy/MoS₂ nanocomposite toward NH₃.

3.9. Sensing Mechanism

The ammonia sensing mechanism of PPy and PPy/MoS₂ nanocomposites is simply explained on the basis of change in electrical conductivity upon adsorption and desorption of analyte at room temperature, as shown in Figure 10a,b. PPy, being a p-type doped conducting polymer, interacts with lone pairs of ammonia which resist the mobility of polarons of PPy, resulting in a decrease in electrical conductivity [9,12]. In case of PPy/MoS₂, the emergence of high electrical conductivity may be due to the interaction of lone pairs of nitrogen of polypyrrole with molybdenum of MoS₂, producing more holes in PPy, leading to a rise in electrical conductivity. As the number of holes increase on PPy, it creates more interaction sites on the polymer with ammonia, leading to high sensitivity of the PPy/MoS₂ nanocomposite.

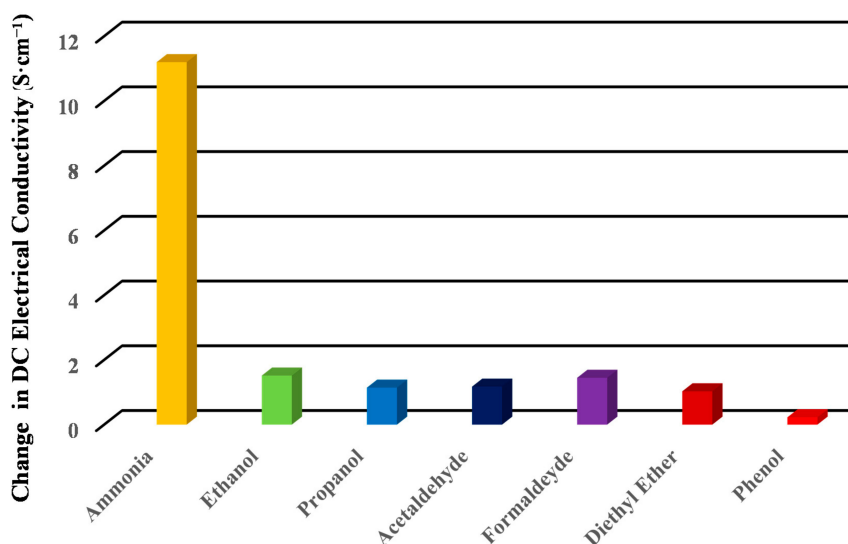
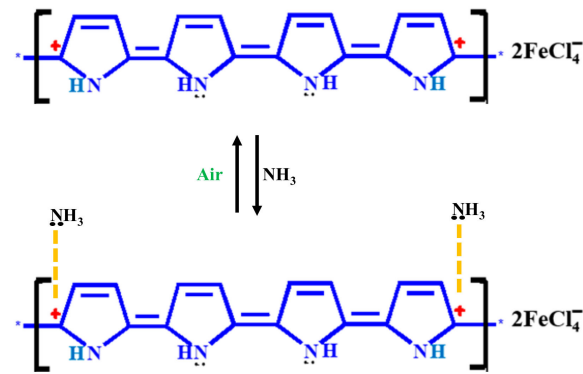


Figure 9. Selectivity of PPy/MoS₂ nanocomposite toward 1000 ppm of ammonia against different 1 M VOCs.

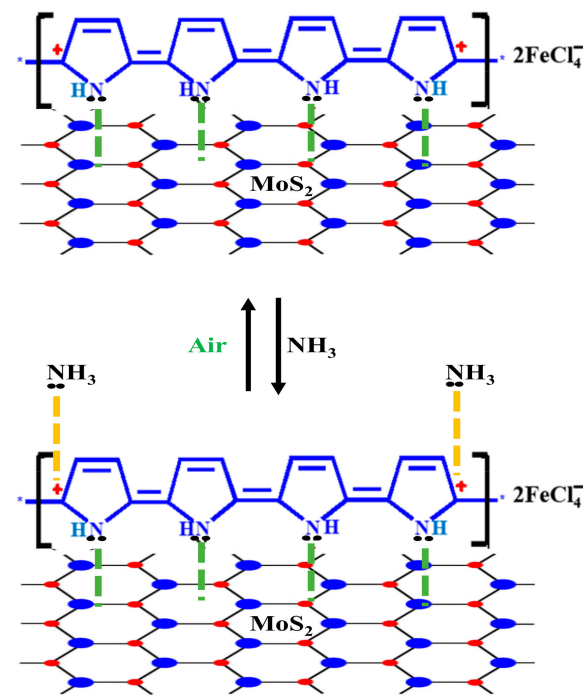
The positive charges on the polypyrrole backbone are polarons (Figure 10a). The main charge carriers in such materials are polarons, besides, protons may also participate in electrical conduction to a very small extent. The main reason for a decrease and increase in electrical conductivity is due to chemisorptions and desorption of ammonia respectively, involving the interaction between the lone pair of ammonia and positive polarons on the polypyrrole backbone. The results show that there is no chemical reaction between ammonia and polypyrrole leading to complete reversibility of electrical conductivity due to un-doping of the polymer [12,30].

As soon as the PPy/MoS₂ nanocomposite is exposed to ambient air, the ammonia molecules get completely detached from the polarons of the PPy/MoS₂ nanocomposite and therefore, the electrical conductivity reverts almost to its initial value (Figure 10b).

The sensing performance of PPy/MoS₂ nanocomposite was compared with other reported work, as shown in Table 1.



(a) PPy



(b) PPy/MoS₂

Figure 10. Schematic representation of the plausible NH₃ adsorption-desorption sensing mechanism on (a) polypyrrole (PPy) and (b) Polypyrrole/MoS₂ (PPy/MoS₂) nanocomposites.

Table 1. Sensing performance of this work (PPy/MoS₂) compared with reported work.

Ammonia Sensing Properties	Co ₃ O ₄ /SnO ₂ [35]	MoS ₂ /ZnO [36]	MOx (SnO ₂ , CuO) Modified rGO [37]	TeO ₂ [38]	SnO ₂ /SWNTs [39]	PANI/α-Fe ₂ O ₃ [40]	PPy/MoS ₂ (This Work)
Response Time	4 s	10 s	100–120 s and 108–132 s	3.1 min	100 s	75 s	60–70 s
Reversibility	17 s	11 s	98–109 s and 98–138 s	5.6 min	3.2 min	5 s	50–60 s
Operating Temperature	200 °C	Room Temperature (RT)	RT	170 °C	RT	RT	RT
Selectivity	Very good	Excellent	Not reported	Not reported	Not reported	Good	Very good

4. Conclusions

PPy and PPy/MoS₂ nanocomposites were successfully synthesized via a chemical oxidative polymerization route. FTIR, XRD and morphological studies proved that the MoS₂ is completely incorporated into the PPy matrix. The PPy/MoS₂ nanocomposite showed very high DC electrical conductivity compared to that of pure PPy. The gas sensing results revealed that the PPy/MoS₂ nanocomposite was found to be an outstanding material for ammonia sensing with quick response and decent selectivity against VOCs. There were about 55 times better variations observed in conductivity of PPy/MoS₂ nanocomposite than that of pure PPy during sensing. Therefore, the PPy/MoS₂ nanocomposite may be a worthwhile, proficient and promising material for ammonia sensing.

Author Contributions: S.A., A.H. and I.K. have synthesized and characterized the samples in detail with the help of A.K., A.M.A. and A.K. did sensitivity parts, and each did a write up of and manuscript formatting and graph fitting. All authors have read and agreed to the published version of the manuscript.

Funding: This research was funded by Deanship of Scientific Research (DSR) at King Abdulaziz University, grant number FP-6-42, and the APC was funded by Deanship of Scientific Research (DSR) at King Abdulaziz University.

Acknowledgments: The Deanship of Scientific Research (DSR) at King Abdulaziz University, Jeddah, Saudi Arabia has funded this project, under grant no. (FP-6-42).

Conflicts of Interest: The authors declare no conflict of interest.

References

1. Shirakawa, H.; Louis, E.J.; MacDiarmid, A.G.; Chiang, C.K.; Heeger, A.J. Synthesis of electrically conducting organic polymers: Halogen derivatives of polyacetylene, (CH)_x. *J. Chem. Soc. Chem. Commun.* **1977**, 578–580. [[CrossRef](#)]
2. Wang, S.R.; Kang, Y.F.; Wang, L.W.; Zhang, H.X.; Wang, Y.S.; Wang, Y. Organic/inorganic hybrid sensors: A review. *Sens. Actuators. B. Chem.* **2013**, *182*, 467–481. [[CrossRef](#)]
3. Bai, H.; Shi, G. Gas Sensors Based on Conducting Polymers. *Sensors* **2007**, *7*, 267–307. [[CrossRef](#)]
4. Pandey, S. Highly Sensitive and Selective Chemiresistor Gas/Vapor Sensors based on Polyaniline Nanocomposite: A comprehensive review. *J. Sci. Adv. Mater. Devices.* **2016**, *1*, 431–453. [[CrossRef](#)]
5. Zhang, Y.; Chen, P.; Wen, F.; Huang, C.; Wang, H. Construction of polyaniline/ molybdenum sulfide nanocomposite: Characterization and its electrocatalytic performance on nitrite. *Ionics* **2016**, *22*, 1095–1102. [[CrossRef](#)]
6. Amirul, M.; Mohd, A.; Syahirah, N.; Razali, M.; Teng, P.; Kulandaivalu, S.; Sulaiman, Y. One-step potentiostatic electrodeposition of polypyrrole/graphene oxide/multi-walled carbon nanotubes ternary nanocomposite for supercapacitor. *Mater. Chem. Phys.* **2018**, *219*, 120–128. [[CrossRef](#)]
7. Jamadade, S.; Jadhav, S.V.; Puri, V. Electromagnetic reflection, shielding and conductivity of polypyrrole thin film electropolymerized in P-Toluenesulfonic acid. *J. Non. Cryst. Solids.* **2011**, *357*, 1177–1181. [[CrossRef](#)]
8. Ahmad, S.; Sultan, A.; Mohammad, F. Rapid response and excellent recovery of a polyaniline/silicon carbide nanocomposite for cigarette smoke sensing with enhanced thermally stable DC electrical conductivity. *RSC Adv.* **2016**, *6*, 59728–59736. [[CrossRef](#)]
9. Sultan, A.; Ahmad, S.; Anwer, T.; Mohammad, F. Binary doped polypyrrole and polypyrrole/boron nitride nanocomposite: Preparation, characterization and application in detection of liquefied petroleum gas leaks. *RSC Adv.* **2015**, *5*, 105980–105991. [[CrossRef](#)]
10. Ansari, M.O.; Mohammad, F. Chemical Thermal stability, Electrical conductivity and ammonia sensing studies on p-toluenesulfonic acid doped polyaniline: Titanium dioxide (pTSA/Pani: TiO₂) nanocomposites. *Sens. Actuators. B. Chem.* **2011**, *157*, 122–129. [[CrossRef](#)]
11. Husain, A.; Ahmad, S.; Mohammad, F. Synthesis, characterisation and ethanol sensing application of polythiophene/graphene nanocomposite. *Mater. Chem. Phys.* **2020**, *239*, 122324. [[CrossRef](#)]
12. Sultan, A.; Mohammad, F. Chemical sensing, thermal stability, electrochemistry and electrical conductivity of silver nanoparticles decorated and polypyrrole enwrapped boron nitride nanocomposite. *Polymer* **2017**, *113*, 221–232. [[CrossRef](#)]

13. Husain, A.; Ahmad, S.; Mohammad, F. Thermally Stable and Highly Sensitive Ethene Gas Sensor Based on Polythiophene/Zirconium Oxide Nanocomposites. *Mater. Today Commun.* **2019**, *20*, 100574. [[CrossRef](#)]
14. Husain, A.; Shariq, M.U.; Mohammad, F. DC electrical conductivity and liquefied petroleum gas sensing application of polythiophene/zinc oxide nanocomposite. *Materialia* **2020**, *9*, 100599. [[CrossRef](#)]
15. Husain, A.; Ahmad, S.; Mohammad, F. Electrical conductivity and alcohol sensing studies on polythiophene/tin oxide nanocomposites. *J. Sci. Adv. Mater. Devices.* **2020**, *5*, 1–11. [[CrossRef](#)]
16. Husain, A.; Ahmad, S.; Mohammad, F. Electrical conductivity and ammonia sensing studies on polythiophene/MWCNTs nanocomposites. *Materialia* **2020**, *14*, 100868. [[CrossRef](#)]
17. Husain, A.; Ahmad, S.; Urooj, M.; Khan, M.M.A. Ultra-sensitive, highly selective and completely reversible ammonia sensor based on polythiophene/SWCNT nanocomposite. *Materialia* **2020**, *10*, 100704. [[CrossRef](#)]
18. Husain, A.; Ahmad, S.; Mohammad, F. Polythiophene/graphene/zinc tungstate nanocomposite: Synthesis, characterization, DC electrical conductivity and cigarette smoke sensing application. *Polym. Polym. Compos.* **2020**, 1–12. [[CrossRef](#)]
19. Tenne, R.; Margulis, L.; Genut, M.; Hodes, G. Polyhedral and cylindrical structures of WS₂. *Nature* **1992**, *360*, 444–446. [[CrossRef](#)]
20. Gopalakrishnan, D.; Damien, D.; Shaijumon, M.M. MoS₂ quantum dot-interspersed exfoliated MoS₂ nanosheets. *ACS Nano.* **2014**, *8*, 5297–5303.
21. Gan, X.; Zhao, H.; Quan, X. Two-dimensional MoS₂: A promising building block for bio sensors. *Biosens. Bioelectron.* **2017**, *89*, 56–71. [[CrossRef](#)] [[PubMed](#)]
22. Vattikuti, S.V.P.; Byon, C. Synthesis and Characterization of Molybdenum Disulfide Nanoflowers and Nanosheets. *Nanotribol. J. Nanomater* **2015**, 1–11. [[CrossRef](#)]
23. Lalithambika, K.C.; Shanmugapriya, K.; Sriram, S. Photocatalytic activity of MoS₂ nanoparticles: An experimental and DFT analysis. *Appl. Phys. A Mater. Sci. Process.* **2019**, *125*, 1–8. [[CrossRef](#)]
24. Ahmad, H.; Ismail, M.A.; Suthaskumar, M.; Tiu, Z.C.; Harun, S.W.; Zulkifli, M.Z.; Samikannu, S.; Sivaraj, S. S-band Q-switched fiber laser using molybdenum disulfide (MoS₂) saturable absorber. *Laser. Phys. Lett.* **2016**, *13*. [[CrossRef](#)]
25. Li, X.; Zhu, H. Two-dimensional MoS₂: Properties, preparation, and applications. *J. Mater.* **2015**, *1*, 33–44. [[CrossRef](#)]
26. Mak, K.F.; Lee, C.; Hone, J.; Shan, J.; Heinz, T.F. Atomically thin MoS₂: A new direct-gap semiconductor. *Phys. Rev. Lett.* **2010**, *105*, 136805. [[CrossRef](#)]
27. Dunlop, M.J.; Bissessur, R. Nanocomposites based on graphene analogous materials and conducting polymers: A review. *J. Mater. Sci.* **2020**, *55*, 6721–6753. [[CrossRef](#)]
28. Lyle, E.S.; McAllister, C.; Dahn, D.C.; Bissessur, R. Exfoliated MoS₂–Polyaniline Nanocomposites: Synthesis and Characterization. *J. Inorg. Organomet. Polym. Mater.* **2020**, *30*, 206–213. [[CrossRef](#)]
29. Lin, B.Z.; Ding, C.; Xu, B.H.; Chen, Z.J.; Chen, Y.L. Preparation and characterization of polythiophene/molybdenum disulfide intercalation material. *Mater. Res. Bull.* **2009**, *44*, 719–723. [[CrossRef](#)]
30. Ahmad, S.; Mujahid, M.; Mohammad, F. Graphene/Nickel Oxide-Based Nanocomposite of Polyaniline with Special Reference to Ammonia Sensing. *ACS Omega* **2018**, *3*, 9378–9387. [[CrossRef](#)]
31. Niaz, N.A.; Shakoor, A.; Imran, M.; Khalid, N.R.; Hussain, F.; Kanwal, H.; Maqsood, M.; Afzal, S. Enhanced electrochemical performance of MoS₂/PPy nanocomposite as electrodes material for supercapacitor applications. *J. Mater. Sci. Mater. Electron* **2020**, *31*, 11336–11344. [[CrossRef](#)]
32. Lian, M.; Wu, X.M.; Wang, Q.G.; Zhang, W.Z.; Wang, Y. Hydrothermal synthesis of Polypyrrole/MoS₂ intercalation composites for supercapacitor electrodes. *Ceram. Int.* **2017**, *43*, 9877–9883. [[CrossRef](#)]
33. Lei, J.Y.; Lu, X.F.; Nie, G.D.; Jiang, Z.Q.; Wang, C. One-Pot Synthesis of Algae-Like MoS₂/PPy Nanocomposite: A Synergistic Catalyst with Superior Peroxidase-Like Catalytic Activity for H₂O₂ Detection. *Part. Part. Syst. Charact.* **2015**, *32*, 886–892. [[CrossRef](#)]
34. Evie, L.P.; Davide, M.; Mirko, P.; Alessandro, B.; Athanassia, A.; Ilker, S.B. An efficient pure polyimide ammonia sensor. *J. Mater. Chem. C.* **2016**, *4*, 7790–7797. [[CrossRef](#)]
35. Wang, L.; Lou, Z.; Zhang, R.; Zhou, T.; Deng, J.; Zhang, T. Hybrid Co₃O₄/SnO₂ Core–Shell Nanospheres as Real-Time Rapid-Response Sensors for Ammonia Gas. *ACS Appl. Mater. Interfaces* **2016**, *8*, 6539–6545. [[CrossRef](#)]

36. Zhang, D.; Jiang, C.; Sun, Y. Room-temperature high-performance ammonia gas sensor based on layer-by-layer self-assembled molybdenum disulfide/zinc oxide nanocomposite film. *J. Alloys Compd.* **2017**, *698*, 476–483. [[CrossRef](#)]
37. Zhang, D.; Liu, J.; Jiang, C.; Liu, A.; Xia, B. Quantitative detection of formaldehyde and ammonia gas via metal oxide-modified graphene-based sensor array combining with neural network model. *Sens. Actuators B Chem.* **2017**, *240*, 55–65. [[CrossRef](#)]
38. Siciliano, T.; Di Giulio, M.; Tepore, M.; Filippo, E.; Micocci, G.; Tepore, A. Ammonia sensitivity of rf sputtered tellurium oxide thin films. *Sens. Actuators B Chem.* **2009**, *138*, 550–555. [[CrossRef](#)]
39. Duc Hoa, N.; Van Quy, N.; Suk Cho, Y.; Kim, D. Nanocomposite of SWNTs and SnO₂ fabricated by soldering process for ammonia gas sensor application. *Phys. Status Solidi (A) Appl. Mater.* **2007**, *6*, 1820–1824. [[CrossRef](#)]
40. Bandgar, D.K.; Navale, S.T.; Naushad, M.; Mane, R.S.; Stadler, F.J.; Patil, V.B. Ultra-sensitive polyaniline–iron oxide nanocomposite room temperature flexible ammonia sensor. *RSC. Adv.* **2015**, *5*, 68964–68971. [[CrossRef](#)]

Publisher’s Note: MDPI stays neutral with regard to jurisdictional claims in published maps and institutional affiliations.



© 2020 by the authors. Licensee MDPI, Basel, Switzerland. This article is an open access article distributed under the terms and conditions of the Creative Commons Attribution (CC BY) license (<http://creativecommons.org/licenses/by/4.0/>).